







Article

Exo⇌*Endo* Isomerism, MEP/DFT, XRD/HSA-Interactions of 2,5-Dimethoxybenzaldehyde: Thermal, 1BNA-Docking, Optical, and TD-DFT Studies

Nabil Al-Zaqri ^{1,*} , Mohammed Suleiman ², Anas Al-Ali ¹ , Khaled Alkanad ³ , Karthik Kumara ⁴ , Neartur K. Lokanath ³, Abdelkader Zarrouk ⁵ , Ali Alsalmeh ¹ , Fahad A. Alharthi ¹, Afnan Al-Taleb ¹, Amjad Alsyaqi ¹ and Ismail Warad ^{2,*}

- ¹ Department of Chemistry, College of Science, King Saud University, P.O. Box 2455, Riyadh 11451, Saudi Arabia; anas.alali@najah.edu (A.A.-A.); aalsalmeh@ksu.edu.sa (A.A.); fharthi@ksu.edu.sa (F.A.A.); afnan1taleb@gmail.com (A.A.-T.); 438203007@student.ksu.edu.sa (A.A.)
- ² Department of Chemistry, Science College, An-Najah National University, Nablus P.O. Box 7, Palestine; suleimanshtaya@najah.edu
- ³ Department of Studies in Physics, University of Mysore, Manasagangotri, Mysore 570006, India; warad@najah.edu (K.A.); lokanath@physics.uni-mysore.ac.in (N.K.L.)
- ⁴ Department of Physics, School of Sciences, Block-I, JAIN (Deemed-to-be University), Bengaluru 560011, India; kk.phy21@gmail.com
- ⁵ Laboratory of Materials, Nanotechnology and Environment, Mohammed V University, Faculty of Sciences, 4Av. Ibn Battuta, Rabat P.O. Box 1014, Morocco; azarrouk@gmail.com
- * Correspondence: nalzaqri@ksu.edu.sa (N.A.-Z.); i.kh.warad@gmail.com (I.W.)

Academic Editor: Reinhard Karl Kremer

Received: 8 November 2020; Accepted: 11 December 2020; Published: 16 December 2020



Abstract: The *exo*⇌*endo* isomerization of 2,5-dimethoxybenzaldehyde was theoretically studied by density functional theory (DFT) to examine its favored conformers via sp^2 – sp^2 single rotation. Both isomers were docked against 1BNA DNA to elucidate their binding ability, and the DFT-computed structural parameters results were matched with the X-ray diffraction (XRD) crystallographic parameters. XRD analysis showed that the *exo*-isomer was structurally favored and was also considered as the kinetically preferred isomer, while several hydrogen-bonding interactions detected in the crystal lattice by XRD were in good agreement with the Hirshfeld surface analysis calculations. The molecular electrostatic potential, Mulliken and natural population analysis charges, frontier molecular orbitals (HOMO/LUMO), and global reactivity descriptors quantum parameters were also determined at the B3LYP/6-311G(d,p) level of theory. The computed electronic calculations, i.e., TD-SCF/DFT, B3LYP-IR, NMR-DB, and GIAO-NMR, were compared to the experimental UV–Vis., optical energy gap, FTIR, and ¹H-NMR, respectively. The thermal behavior of 2,5-dimethoxybenzaldehyde was also evaluated in an open atmosphere by a thermogravimetric–derivative thermogravimetric analysis, indicating its stability up to 95 °C.

Keywords: *exo*⇌*endo* isomerism; docking; density functional theory; thermal stability; X-ray diffraction; 2,5-dimethoxybenzaldehyde

1. Introduction

Aldehydes and ketones are key building blocks for a wide range of synthetic and natural derivatives and are used in several applications such as the Schiff base reaction [1–4]. In particular, aldehydes are commonly used for the development of effective drugs due to their several biological activities resulting

from the polar HC=O group [4–6]. Nevertheless, improvements in density functional theory (DFT) methods have allowed the reliable theoretical application of larger molecules with even more 100 atoms in the development of new pharmaceutical agents. Therefore, DFT is currently the most powerful tool for quantum chemistry computations [7–10] and, along with X-ray single crystal analysis, has become particularly valuable for structural optimizations [9–12]. Moreover, DFT has significantly contributed in the evaluation and comparison of several experimental spectral analyses [11–13]. Molecular docking is also a suitable method for understanding the binding mode of drugs with DNA via, e.g., noncovalent interactions [14–18], and is usually applied for the design of novel drug structures. Besides, both experimental and theoretical docking studies help to explore organic and inorganic complexes as potential drug candidates [18].

A literature survey revealed that the *exo*↔*endo* isomerization of 2,5-dimethoxybenzaldehyde at the DFT/B3LYP level of theory, as well as quantum computations that have not yet been performed. Therefore, in this study, the structure of the isomerization transition state was estimated by the QST2 method. The X-ray diffraction (XRD) structure of the *exo*-isomer was identified as the kinetically favored isomer, indicating that the structure parameters determined by XRD and DFT studies were in good agreement. To establish the intermolecular forces in the crystal lattice, the results of the Hirshfeld surface analysis (HSA) and molecular electrostatic potential (MEP) computations were compared with the experimental XRD packing results. In addition, the MEP, Mulliken and natural population analysis (NPA) charges, frontier molecular orbital (HOMO/LUMO), and global reactivity descriptor (GRD) quantum parameters were determined, while the computed electronic calculations (TD-SCF/DFT/B3LYP, GIAO-NMR, and DFT-IR) were matched to UV–Vis, the optical energy gap (E_g), FTIR, and ^1H NMR experimental spectra, respectively, under identical conditions. Moreover, the *exo*- and *endo*-isomers of 2,5-dimethoxybenzaldehyde could be sufficiently reflected, docked against one DNA helix DNA through the development of two strong hydrogen bonds.

2. Experimental Section

2.1. Computational Methodology

In order to determine the optimization, Mulliken, NPA, HOMO/LUMO, GRD, TD-SCF/DFT, B3LYP-IR, NMR-DB, and GIAO-NMR quantum-chemical parameter calculations of the desired molecule in a gaseous phase have been performed using Becke's three parameter exchange function (B3) with the Lee-Yang-Parr correlation function (LYP) with basis sets 6-311G(d,p) [19–21]. The DFT/B3LYP/6-311G(d,p) level of theory is found to be very suitable for pure organic compounds like the desired molecule in this study [21]. Moreover, the QST2 computation method was applied to detect the transition state (TS) of the *exo*↔*endo* isomerization reaction [21].

2.2. XRD and HSA

CrystalExplorer 3.1 was used for the HSA analysis [22] using a colorless $0.29 \times 0.26 \times 0.23$ -mm single crystal of *exo*-2,5-dimethoxybenzaldehyde. The structure was solved using the SHELXL and SHELXS programs [23]. Crystal refined parameters are illustrated in Table 1.

Table 1. Crystallographic refined parameters of the desired molecular structure.

Empirical Formula	C ₉ H ₁₀ O ₃
CCDC	1860213
Temperature	293(2) K
Formula weight	166.17
Wavelength	0.71073 Å
Crystal system, space group	Monoclinic, p21/n
Volume	639.55(5) Å ³
Unit cell dimensions	a = 3.9469 (9), b = 11.580 (3), c = 17.886 (4) Å
β	91.442 (17)°
V	817.2 (3) (Å) ³
Crystal size	0.29 × 0.26 × 0.23 mm
Z	4
Absorption coefficient	0.1 mm ⁻¹
No. of reflections	1837
Refinement method	Full-matrix least-squares on F ²
R(int), (sin θ/λ) _{max}	0.115, 0.650 (Å ⁻¹)
S	1.05
R[F ₂ > 2σ(F ₂)], wR(F ₂)	0.062, 0.190
Largest diff. peak and hole	0.14, -0.20 eÅ ⁻³

2.3. 2,5-Dimethoxybenzaldehyde Crystallization

In order to obtain suitable crystals for XRD measurements, 100 mg of commercially available 2,5-dimethoxybenzaldehyde (C₉H₁₀O₃, Aldrich, St. Louis, MO, USA, 99.0% pure) (100 mg) was dissolved in 10-mL MeOH at room temperature. After 2 days of evaporation at this temperature, colorless crystals were slowly formed.

2.4. BNA Docking

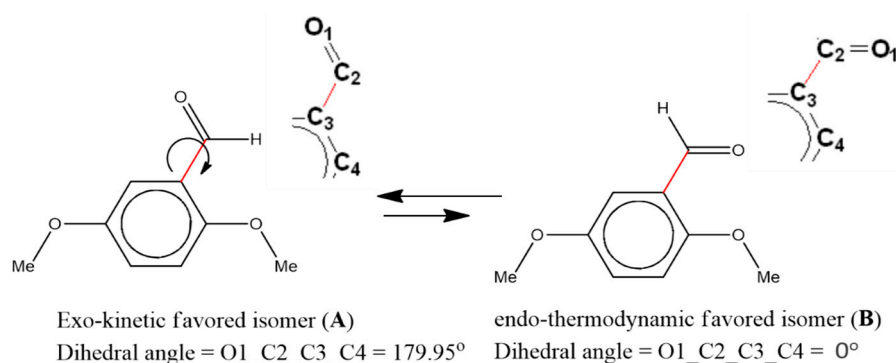
Docking studies were performed using the Autodock4.2 running on an Intel(R) Core(TM) i5 CPU (3 GHz) processor with a Windows 2007 operating system, Palo Alto, California, USA. The isomer structures were prepared using ChemDraw. The docking was performed using the Gasteiger charges, the water molecules were erased, and the nonpolar hydrogen atoms were merged using AutoDock4 [24]. The X-ray crystal of PDB ID: 1BNA DNA was freely obtained from the Protein Data Bank [25].

3. Results and Discussion

3.1. XRD and DFT Structure Analysis

XRD analysis indicated that *exo*-2,5-dimethoxybenzaldehyde (**A**) was the kinetically favored isomer with a dihedral angle ($\tau_{O1-C2-C3-C4}$) of 179.95°. In contrast, the thermodynamically favored *endo*-isomer (**B**) with $\tau_{O1-C2-C3-C4} = 0^\circ$ was not detected by XRD (Scheme 1).

2,5-Dimethoxybenzaldehyde crystallized in the kinetically favored *exo*-isomer form (Figure 1a) was monoclinic, with a p21/n space group, and four molecules were crystallized in a packing unit cell (Figure 1b). In the gaseous phase, the B3LYP/6-311G(d,p)-optimized *exo*-isomer structure was consistent with the XRD experimental result of the solid state, as shown in Figure 1c and Table 2.



Scheme 1. *Exo*⇌*endo* isomerization of 2,5-dimethoxybenzaldehyde and the O1–C2–C3–C4 dihedral angles of the corresponding isomers.

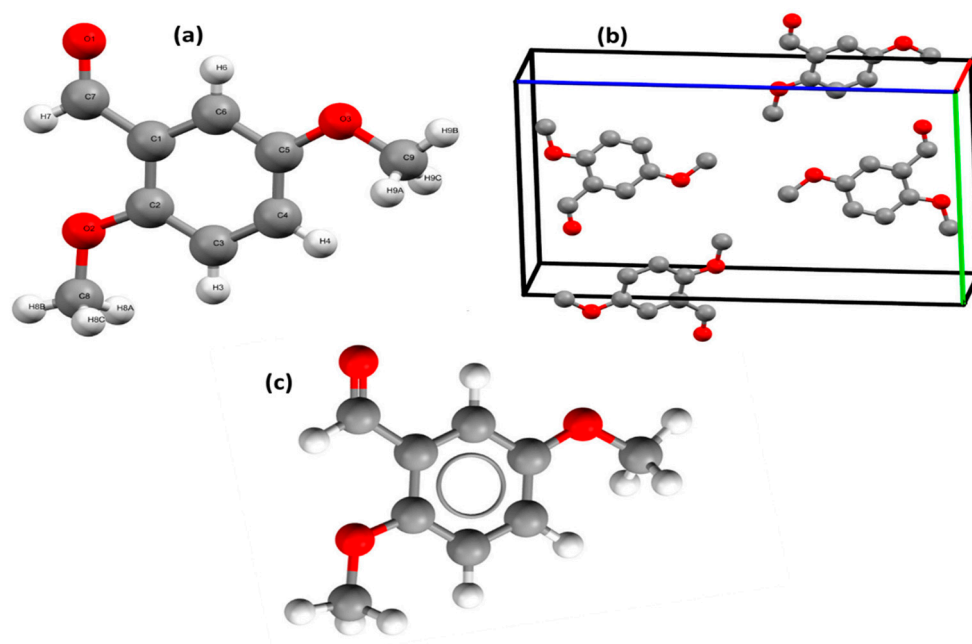


Figure 1. (a) ORTEP drawing of *exo*-2,5-dimethoxybenzaldehyde. (b) Packing unit cell with four crystallized *exo*-2,5-dimethoxybenzaldehyde molecules. (c) B3LYP/6-311G(d,p)-optimized structure of *exo*-2,5-dimethoxybenzaldehyde.

Table 2. Density functional theory (DFT)-calculated angles (°) and bond lengths (Å) compared to the corresponding X-ray diffraction (XRD) experimental results (exp. XRD).

Bond No.	Bonds	Exp. XRD	DFT	Angle No.	Angles (°)	Exp. XRD	DFT
1	O3 C5	1.371(2)	1.3639	1	C5 O3 C9	117.3(2)	118.73
2	O3 C9	1.409(3)	1.4207	2	C2 O2 C8	117.7(2)	118.38
3	O2 C2	1.364(2)	1.3655	3	C5 C6 C1	120.6(2)	120.56
4	O2 C8	1.410(3)	1.4189	4	O2 C2 C1	116.5(2)	116.62
5	O1 C7	1.197(3)	1.2124	5	O2 C2 C3	123.9(2)	124.35
6	C6 C5	1.379(3)	1.393	6	C1 C2 C3	119.6(2)	119.03
7	C6 C1	1.384(3)	1.3978	7	O3 C5 C6	116.3(2)	116.2
8	C2 C1	1.391(3)	1.4138	8	O3 C5 C4	124.4(2)	124.95
9	C2 C3	1.384(3)	1.3964	9	C6 C5 C4	119.3(2)	119.73
10	C5 C4	1.377(3)	1.3919	10	C5 C4 C3	120.9(2)	120.58
11	C4 C3	1.379(3)	1.3939	11	C6 C1 C2	119.7(2)	120.39
12	C1 C7	1.465(3)	1.4838	12	C6 C1 C7	119.0(2)	118.88
				13	C2 C1 C7	121.3(2)	121.25
				14	C2 C3 C4	119.9(2)	118.84
				15	C1 C7 O1	124.7(2)	123.68

3.2. B3LYP/6-311G(d,p) Structures

The bond distances and angles determined by DFT and XRD were almost identical, as shown in Table 2 and Figure 2. Specifically, the correlation (R^2) between the calculated/experimental bond lengths was found to be 0.9845 (Figure 2a,b) and that between the calculated and experimental angles was 0.9357 (Figure 2c,d). Slight differences were only observed, because the DFT was performed in the gaseous phase, while XRD in the solid state.

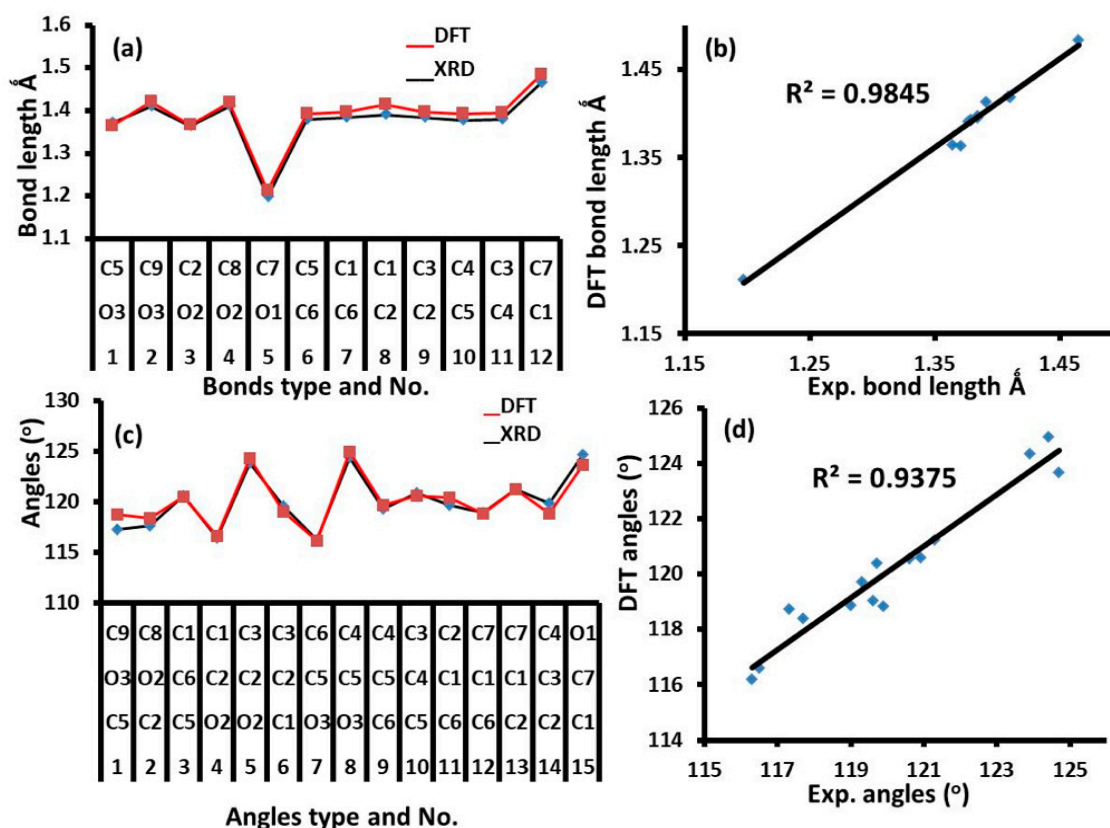


Figure 2. Histograms of (a) bond lengths and (c) angles determined by X-ray diffraction (XRD) and density functional theory (DFT). (b) and (d) Graphical correlations of the bond lengths and angles determined by XRD and DFT, respectively.

3.3. Exo⇌Endo Computational Isomerism

The *exo*-kinetic isomer did not favor the coordination of a metal ion, as the carbonyl oxygen and 2-OCH₃ oxygen atoms were in the opposite direction. Although its structure was sterically favored, it did not serve as a good O∩O bidentate ligand. In contrast, the *endo*-isomer was expected to be a good O∩O bidentate chelate ligand, as the two oxygen atoms were in the same direction. Although the geometry of the *exo*-isomer was not appropriate for ligation, the formation of a stable S6-fused metal–heterocyclic ring after isomerization was confirmed by XRD crystal analysis (Figure 3).

Therefore, here, we investigated the *exo*⇌*endo* isomerization based on theoretical measurements to identify the energy required to switch between the two isomers. As shown in Scheme 1, the stereochemical difference between the two isomers is controlled by a 90° single rotation around the cited C_{sp2}–C_{sp2} single bond, which leads to a significant change in the $\tau_{O_1-C_2-C_3-C_4}$ dihedral angle from 180° (*exo*) to 0° (*endo*). Based on this change, and ignoring all the intermolecular forces in both isomers, high-level DFT/B3LYP/6-311G(d) optimization calculations were performed in the gaseous state for both isomers. Moreover, the QTS2 computation method was applied to detect the transition state (TS) of the *exo*⇌*endo* isomerization reaction (Figure 4).

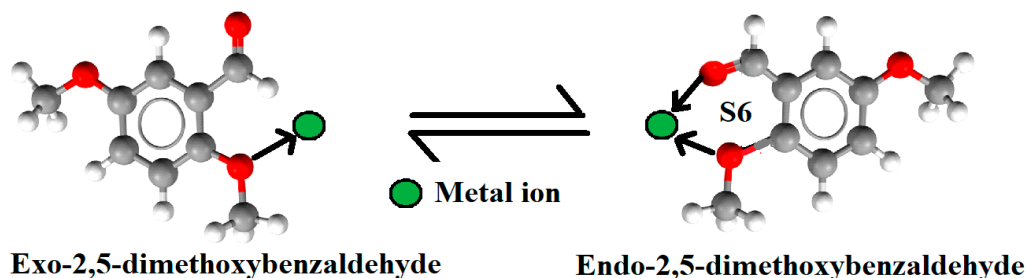


Figure 3. Formation of a S6-fused metal–heterocyclic ring after the *exo*⇌*endo* isomerization of 2,5-dimethoxybenzaldehyde.

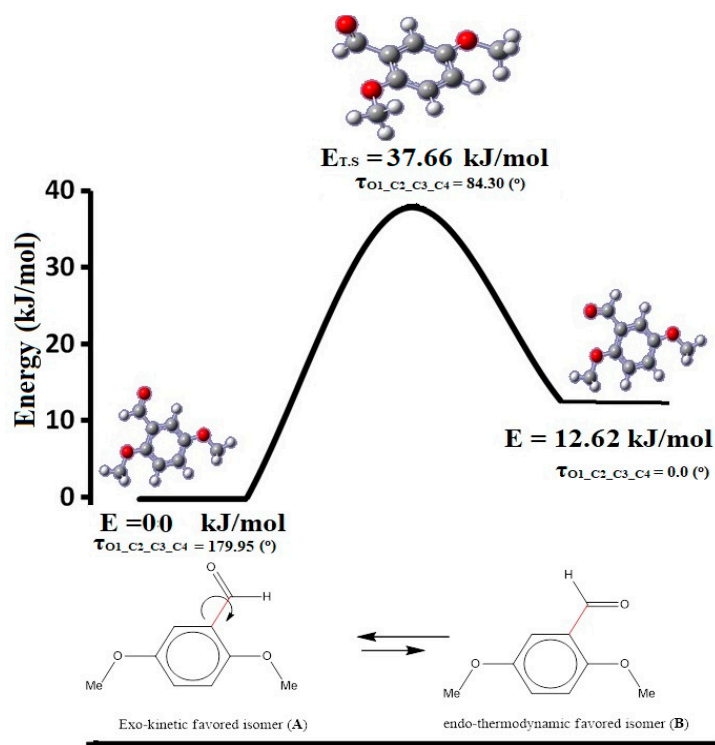


Figure 4. Energy profile and global minimum structures of the *exo*- and *endo*-2,5-dimethoxybenzaldehyde isomers and the transition state (TS) of the *exo*⇌*endo* isomerization.

Based on the energy profile of the *exo*⇌*endo* isomerization of 2,5-dimethoxybenzaldehyde (Figure 4), the *exo*-isomer energy was -574.76611449 a.u., $E_{\text{exo}} = 0.0$ kJ, whereas that of the *endo*-isomer was found at -574.76130900 a.u., $E_{\text{endo}} = 12.62$ kJ. Moreover, the TS energy was higher than that of both isomers (-574.75176736 a.u., $E_{\text{TS}} = 37.66$ kJ), and its structure was between the structure of the *endo*- and *exo*-isomers with a dihedral angle of 84.3° . Therefore, we demonstrated that, energetically, the stable *exo*-isomer could give the unfavorable *endo*-isomer, since the energy required for isomerization was not too high and could be easily provided by the surrounding environment or solvents.

3.4. Crystal Interactions and HSA Investigation

Three main H⋯O hydrogen bond interactions were detected in the crystal lattice of *exo*-2,5-dimethoxybenzaldehyde molecules, while each molecule was bound to its surrounding molecules through six hydrogen bonding interactions (Figure 5a), and no other types of interactions were identified. The two shortest interactions were assigned to the C=O⋯H_{Me} hydrogen-bonding interactions with a distance of 2.669 \AA , forming a semi-dimer S14 supramolecular system (Figure 5b), while two C=O⋯H_{Me} hydrogen bonds with 2.703 \AA (Figure 5c) and two MeO⋯H_{ph} hydrogen bonds with 2.702 \AA (Figure 5d) could also be detected.

During HSA, four red spots were detected on the d_{norm} surface of the computed molecule [26–30], which were all attributed to the formation of H··O hydrogen bonds (Figure 6a). It should be noted that the type and the number of the hydrogen bonds identified by HSA were consistent with those detected by an XRD packing analysis (Figure 6b). In addition, the HSA 2D fingerprint plots over the computed surface molecule indicated the presence of 65.9% total hydrogen interactions, which corresponded to three types of hydrogen-bonding interactions, namely H··H (48.3%) > H··O (13.9%) > H··C (3.7%) (Figure 6c).

3.5. MEP Analysis and Atomic Charge Populations

The MEP analysis suggested the presence of both electrophilic and nucleophilic sites on the molecule surface (Figure 7a). The carbonyl oxygen atom was indicated as the strongest nucleophile site (red), while the other oxygen atoms were less nucleophilic (yellow). Moreover, the phenyl and methyl hydrogen atoms had strong electrophilic positions (blue). These findings strongly supported the formation of H··O hydrogen bonds [31], as already confirmed by the XRD experimental results and HSA computations.

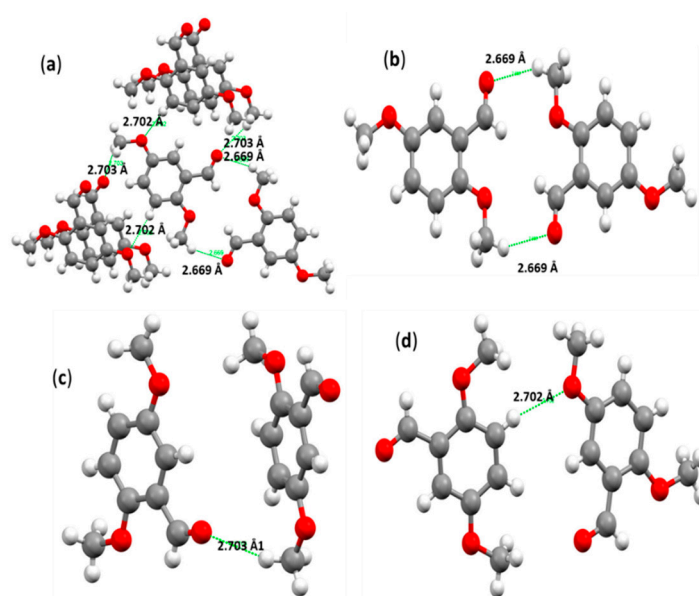


Figure 5. (a) Six hydrogen bond interactions determined in the crystal lattice of *exo*-2,5-dimethoxybenzaldehyde molecules. (b) C=O··H_{Me}: 2.669 Å, (c) C=O··H_{Me}: 2.703 Å, and (d) MeO··H_{ph}: 2.702 Å.

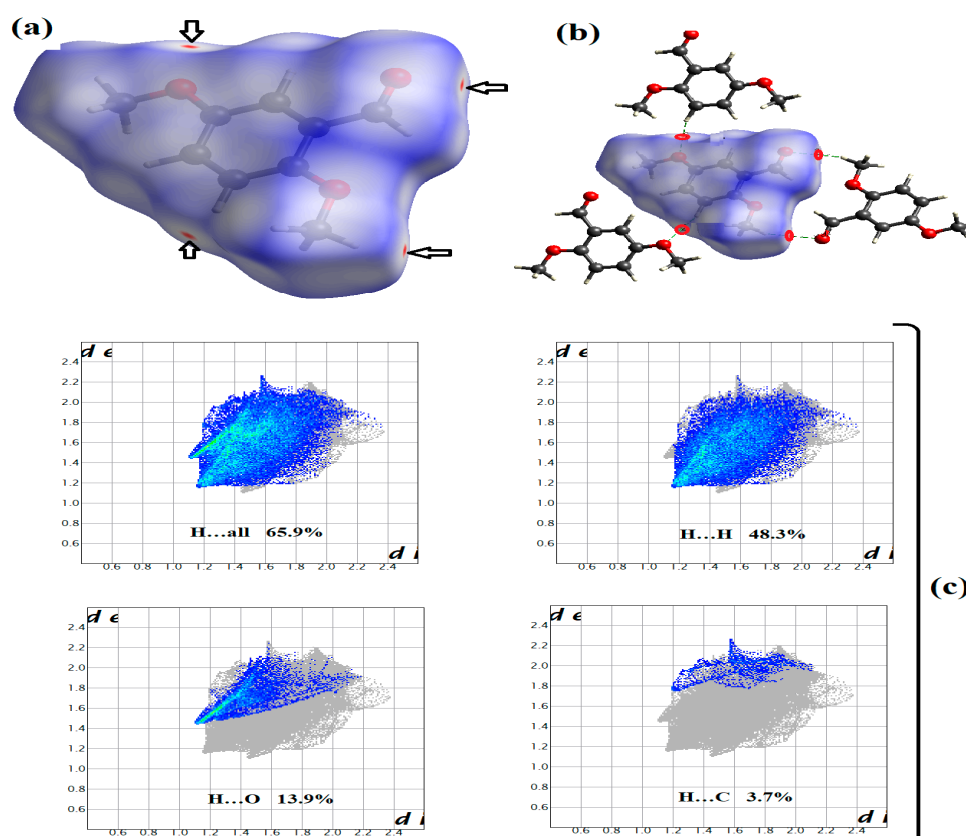


Figure 6. (a) Map of the d_{norm} surface of the computed molecule. (b) Hydrogen bonding interactions of the computed molecule with its neighboring molecules. (c) Hirshfeld surface analysis (HSA) 2D fingerprint plots indicating the H...H, H...O, and H...C hydrogen-bonding interactions.

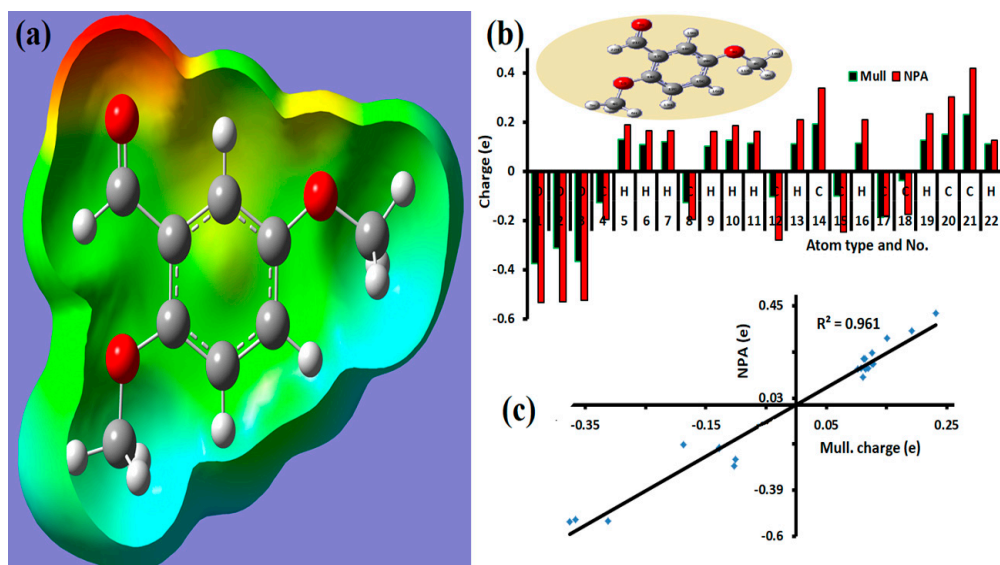


Figure 7. (a) B3LYP/6-311G(d,p) molecular electrostatic potential (MEP) map of *exo*-2,5-dimethoxybenzaldehyde. (b) Mulliken (Mull) and natural population analysis (NPA) atomic charges and (c) their graphical correlation. R^2 : correlation.

The determination of the Mulliken and NPA atomic charges revealed the presence of digital electron-poor and electron-rich atoms (Figure 7b). In general, the NPA atomic charges were higher than the Mulliken atomic charges, while the Mulliken and NPA values confirmed that all the oxygen

atoms, as well as the C4, C8, C12, C15, C17, and C18 carbon atoms, acted as nucleophilic sites (Table 3). Accordingly, the electrophilic sites corresponded to the C13, C14, C20, and C21 carbon atoms. Moreover, all hydrogen atoms showed positive charge values, with H5, H10, and H19 being the most electrophilic (Table 3). A high correlation between Mulliken and NPA charge with $R = 0.9614$ was also observed based on the plot of Figure 7c. It is worth noting that the Mulliken and NPA data were in good agreement with the MEP, XRD packing, and HSA results.

The shape and energy diagram of HOMO and LUMO indicated that the electron donation capacity in the UV region was $\Delta E_{\text{HOMO/LUMO}} = 4.266$ eV (Figure 8a). Moreover, by measuring the B3LYP/6-311G(d,p) electron transfer in the gaseous state and in MeOH and DMSO (Figure 8b), two broad maxima bands at $\lambda_{\text{max}} = 245$ and 355 nm were observed, corresponding mainly to HOMO-2-to-LUMO (76%) and HOMO-to-LUMO (96%) transitions, respectively. Similar electron transition results were obtained by experimental UV spectra, as shown in Figure 8c. Specifically, two peaks with λ_{max} at 250 and 350 nm were detected in MeOH and DMSO, which were assigned to $\pi \rightarrow \pi^*$ and $n \rightarrow \pi^*$ electron transitions, respectively. Moreover, no solvatochromism effect was observed by changing the solvents in both the experimental and theoretical studies. The small $\Delta\lambda$ shift (~ 5 nm) between the experimental and DFT data could be attributed to the solute-solvent interaction [32]. In addition, the experimental optical energy band gap (E_g) in MeOH and DMSO was determined using the Tauc equation [33]. Based also on Figure 8d, the direct E_g value was found to be ~ 4.51 eV in both solvents, which was close to the $\Delta E_{\text{HOMO/LUMO}}$ value (~ 4.3 eV).

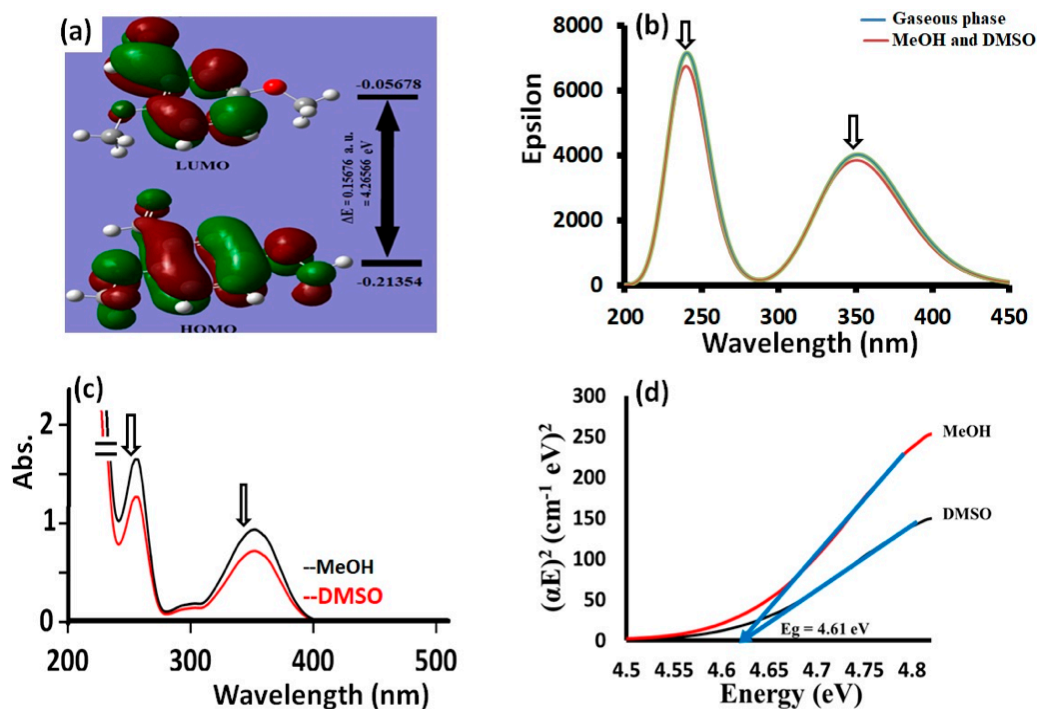


Figure 8. (a) HOMO/LUMO shapes and energy diagram. (b) TD-DFT. (c) Experimental UV spectra, and (d) optical energy band gap (E_g) of the 2.2×10^{-6} M of 2,5-dimethoxybenzaldehyde in MeOH and DMSO.

Table 3. Mulliken (Mull) and natural population analysis (NPA) atomic charges.

Atom No.	Atom	Mull	NPA	Atom No.	Atom	Mull	NPA
1	O	-0.37563	-0.53238	12	C	-0.10245	-0.27906
2	O	-0.31227	-0.53113	13	H	0.111993	0.2103
3	O	-0.36585	-0.5234	14	C	0.191826	0.33756
4	C	-0.12813	-0.19544	15	C	-0.10028	-0.24795
5	H	0.128088	0.1876	16	H	0.113917	0.20922
6	H	0.107874	0.16505	17	C	-0.1867	-0.18217
7	H	0.11955	0.16505	18	C	-0.03829	-0.17568
8	C	-0.12758	-0.19749	19	H	0.126519	0.23468
9	H	0.102642	0.16179	20	C	0.151051	0.30193
10	H	0.126294	0.18724	21	C	0.23168	0.41763
11	H	0.115255	0.16178	22	H	0.110488	0.12487

HOMO-LUMO, TD-SCF-B3LYP, absorbance, optical energy gap (E_g), and global reactivity descriptors (GRD).

The GRD quantum parameters of the ligand, including softness (σ), hardness (η), chemical potential (μ), electrophilicity (ω), and electronegativity (χ), were also calculated by the following equations (Table 4):

$$I: \text{ Ionization potential} = -E_{HOMO} \quad (1)$$

$$A: \text{ Electron affinity} = -E_{LUMO} \quad (2)$$

$$\Delta E_{gap}: \text{ Energy gap} = E_{HOMO} - E_{LUMO} \quad (3)$$

$$\chi: \text{ Absolute electronegativity} = (I + A)/2 \quad (4)$$

$$\eta: \text{ Global hardness} = (I - A)/2 \quad (5)$$

$$\sigma: \text{ Global softness} = 1/\eta \quad (6)$$

$$\mu: \text{ Chemical potential} = -\chi \quad (7)$$

$$\omega: \text{ Electrophilicity} = \mu^2/2\eta \quad (8)$$

Table 4. Global reactivity descriptor (GRD) quantum parameters calculated for *exo*-2,5-dimethoxybenzaldehyde.

GRD		Value
Global total energy	E_T	-574.76611449 a.u.
Low unoccupied molecular orbital	<i>LUMO</i>	-0.05678 a.u.
High occupied molecular orbital	<i>HOMO</i>	-0.21354 a.u.
Energy difference	ΔE_{gap}	0.15676 a.u. 4.26565 eV
Electron affinity	<i>A</i>	1.545063 eV
Ionization potential	<i>I</i>	5.810721 eV
Global hardness	η	2.13505 eV
Global softness	σ	0.468372 eV
Chemical potential	μ	-3.67789 eV
Electronegativity	χ	3.67789 eV
Electrophilicity	ω	3.16781 eV
Dipole moment	<i>u</i>	6.4226 D

3.6. FTIR Investigations

The experimental FTIR spectrum of 2,5-dimethoxybenzaldehyde in a solid state indicated the presence of several functional groups, which were consistent with its chemical formula. In particular, the peaks at ~ 3050 , 2950–2840, and 1620 cm^{-1} were attributed to the C–H_{ph}, C–H_{CH₃}, and C=O stretching vibrations, respectively (Figure 9a). Moreover, it is clear from Figure 9b that the experimental

and DFT-calculated spectra were very similar, while their high compatibility was further confirmed by their excellent correlation with $R^2 = 0.998$ (Figure 9c).

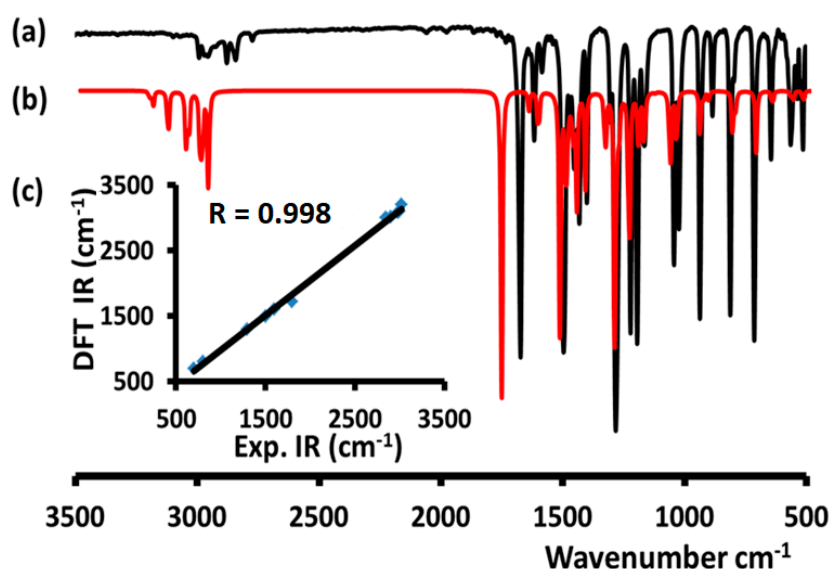


Figure 9. (a) Experimental and (b) DFT-calculated FTIR spectra of 2,5-dimethoxybenzaldehyde, and (c) their graphical correlation.

3.7. Computed and Experimental ^1H NMR

The experimental ^1H -NMR spectrum of 2,5-dimethoxybenzaldehyde was recorded in CDCl_3 (Figure 10a). In the aliphatic region, two broad peaks were detected at 3.65 and 3.76 ppm corresponding to OCH_3 , while the peaks at 6.91 (*d*), 7.11 (*d*), and 7.31 (*s*) ppm were assigned to the three aromatic protons. The aldehyde proton was detected at 10.45 ppm as a singlet. The theoretical NMR-DB [16] (Figure 10b) and GIAO-NMR (Figure 10c) in CDCl_3 were similar to the experimental spectrum, while the calculated and experimental proton chemical shifts showed a very good correlation, with R^2 values of 0.9975 and 0.9929, respectively.

3.8. Molecular Docking

Both *exo*- and *endo*-isomers of 2,5-dimethoxybenzaldehyde were docked to DNA (PDB ID: 1BNA) under the same level of theory based on the existing data [25]. Interestingly, both isomers showed good and similar docking behaviors and were cross-linked to one DNA helix via two hydrogen bonds to form a (DNA:isomer) complex. No π - π stacking interactions were observed (Figure 11), while the polar 3- OCH_3 functional group of both isomers did not develop hydrogen-bonding interactions with DNA, as it did not interfere with the DNA helix in the crystal lattice, which supported the minor groove DNA intercalation.

In addition, the binding affinity of the *exo*-isomer indicated its close contact with the DNA surface through a minor groove intercalation mode (Figure 11a) and two short hydrogen bonds to the adenosines of the one DNA helix (Figure 11b). The hydrogen-bonding interactions were assigned to DNA DA17: $\text{H}\cdots\text{OMe}$ (ligand) with 1.984 Å and DNA DA18: $\text{H}\cdots\text{O}=\text{C}$ (ligand) with 1.665 Å (Figure 11c). The docking results were consistent with the hydrogen bonds detected in the crystal lattice of the solved structure. In general, the docking effect can be considered a good result when the root mean square deviation (RMSD) value is below 2 Å [32]. The theoretical binding constant (K_b) and free energy change for the *exo*-isomer were found to be 1.63×10^4 and -5.72 kcal/mol, respectively.

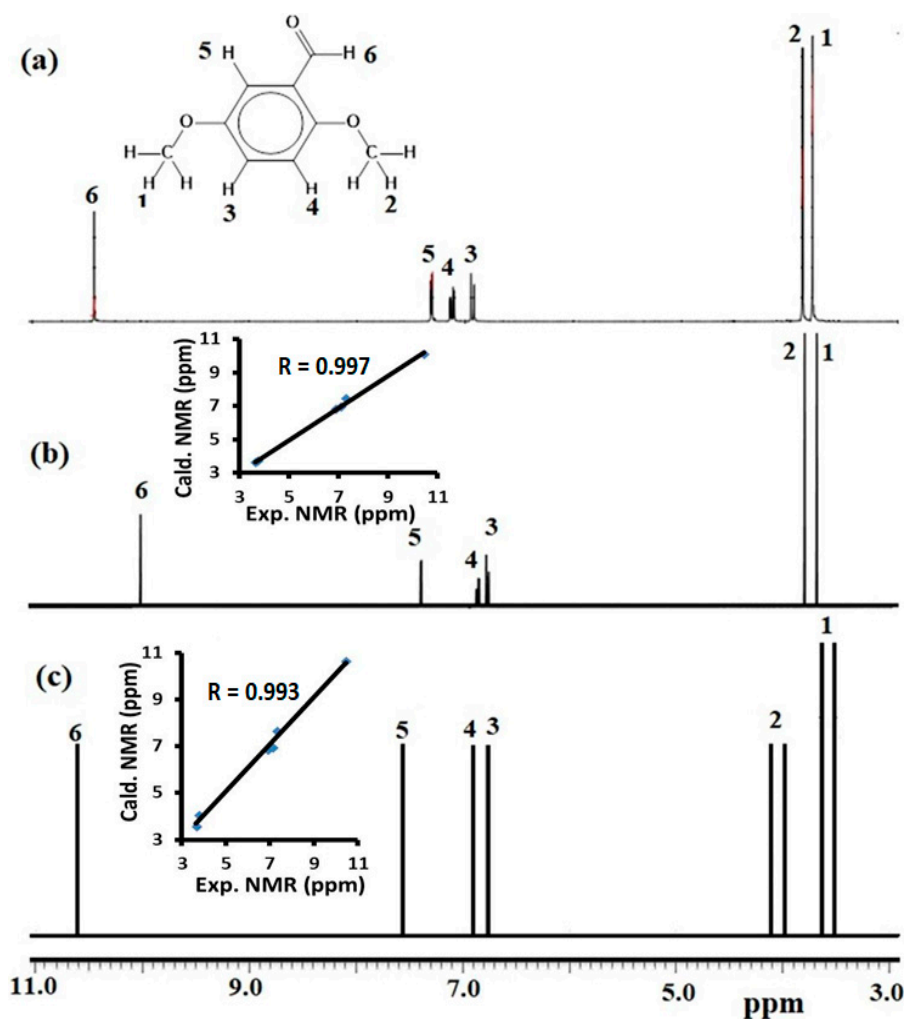


Figure 10. (a) Experimental ^1H NMR spectrum of 2,5-dimethoxybenzaldehyde in CDCl_3 . Theoretical (b) NMR-DB and (c) GIAO-NMR spectrum of 2,5-dimethoxybenzaldehyde in CDCl_3 .

Similar to the *exo*-isomer, the *endo*-isomer was also in contact with DNA via a minor groove intercalation mode (Figure 12a), and one helix binding was observed (Figure 12b). However, this isomer developed two longer hydrogen-bonding interactions with the DNA adenosines, i.e., DA17:H \cdots OME (ligand) with 2.481 Å and DNA DA18:H \cdots O=C (ligand) with 1.927 Å (Figure 12c). According to the RMSD, one bond was considered to be a good interaction. The theoretical K_b and free energy change were determined at 1.10×10^4 and -5.49 kcal/mol, respectively.

The study showed significant convergence in the docking behavior of both isomers. However, the *exo*-isomer seemed to be slightly more active than the *endo*-isomer, since its hydrogen bonds were stronger, and its binding energy and K_b values were higher. These results could be expected, as the *exo*-isomer is more stable, and its structural shape selectivity is more suitable for structure-based drug discovery [16].

3.9. Thermal Analysis

The thermal properties of 2,5-dimethoxybenzaldehyde were also evaluated by thermogravimetric–derivative thermogravimetric (TG/DTG) analysis. The TG/DTG curves were obtained at a temperature range of 0–300 °C at a heating rate of 5 °C/min in an open atmosphere (Figure 13). The ligand exhibited acceptable stability up to = 95 °C, while, at temperatures above 95 °C, the ligand was gradually decomposed, and its weight decreased from 100 wt% to 0 wt% via a single broad-step reaction mechanism with $T_{\text{off}} \approx 200$ °C and complete thermal decomposition.

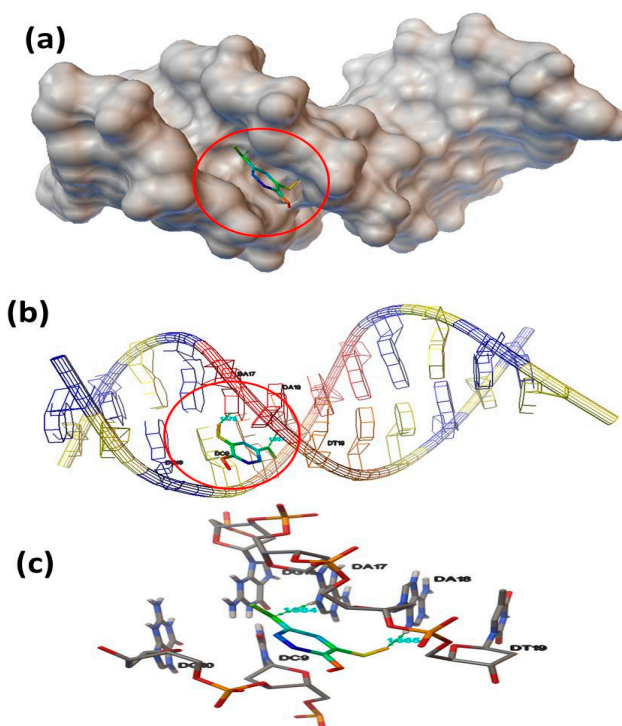


Figure 11. (a) Schematic representation of the binding position of the *exo*-isomer to DNA. (b) Interactions of the *exo*-isomer with the nucleides of the one DNA helix. (c) Hydrogen-bonding interactions of the *exo*-isomer with DNA adenosines (DA17: H...OMe and DA18: H...O=C).

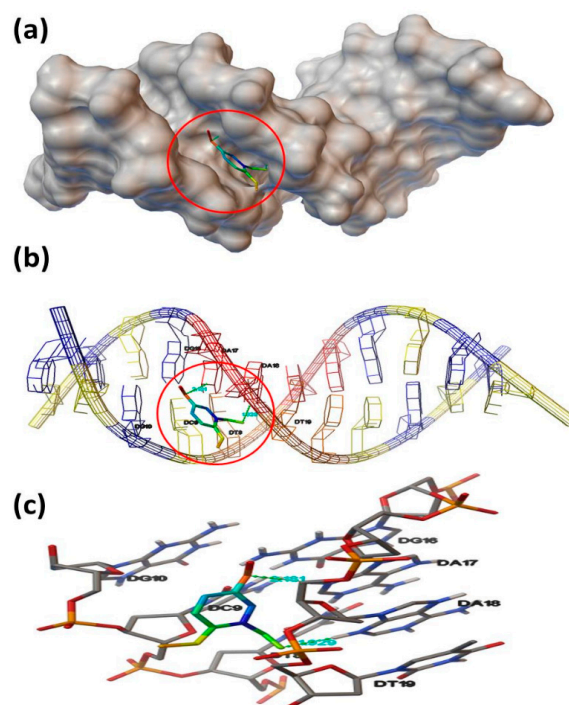


Figure 12. (a) Schematic representation of the binding position of the *endo*-isomer to DNA. (b) Interactions of the *endo*-isomer with the nucleides of the one DNA helix. (c) Nuclides-Z-isomer positional binding and hydrogen-bonding interactions of the *exo*-isomer with DNA adenosines (DA17: H...OMe and DA18: H...O=C).

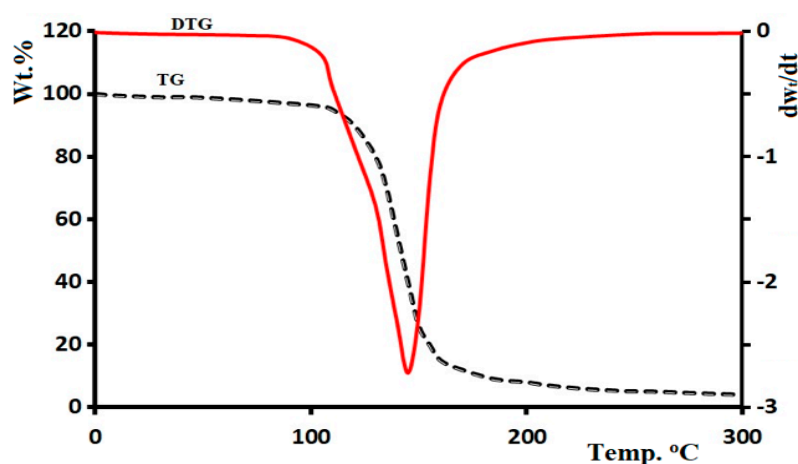


Figure 13. Thermogravimetric–derivative thermogravimetric (TG/DTG) curves of 2,5-dimethoxybenzaldehyde.

4. Conclusions

In this study, we explored the *exo*⇌*endo* isomerization of 2,5-dimethoxybenzaldehyde based on DFT studies, and the results were compared and confirmed by experimental studies. The formation of the *exo*-isomer was confirmed by the XRD crystallographic analysis structure, while the DFT/XRD structure parameters reflected semi-unity graphical correlations. The hydrogen bonds computed by HSA and MEP analyses were in excellent agreement with the experimental XRD packing results, while the Mulliken and NPA population charge analyses indicated the presence of both nucleophilic and electrophilic sites on the ligand surface. Moreover, the DFT/B3LYP/6-311G(d,p) computational study of the *exo*⇌*endo* isomerization process allowed the identification of the QST2 TS. Furthermore, the TD-SCF/DFT, B3LYP-IR, NMR-DB, and GIAO-NMR calculations were similar to the experimental UV–Vis, direct E_g , FTIR, and ^1H NMR spectra, respectively. The calculated Mulliken and NPA population charges, along with the HOMO/LUMO and GRD quantum parameters, further supported the *exo*-isomer formation. The ligand also exhibited good thermal stability, with a one-step decomposition mechanism in the range of 100–200 °C. In addition, both isomers showed a very good DNA docking effect, where one helix minor groove with two hydrogen bonds was observed for both isomers. Such compounds can be used in future works as DNA-binding promising drugs.

Author Contributions: Data curation: N.A.-Z. and I.W.; formal analysis: M.S.; funding acquisition: N.A.-Z. and A.A. (Amjad Alsyahi); investigation: A.A.-A., K.A., and N.K.L.; methodology: A.Z., F.A.A., and A.A.-T.; project administration: N.A.-Z. and A.A. (Ali Alsalmeh), software: I.W.; validation: N.A.-Z.; writing—original draft: I.W. and A.A.-A.; writing—review and editing: K.K., N.K.L., A.Z., and M.S. All authors have read and agreed to the published version of the manuscript.

Funding: The authors extend their appreciation to the Deputyship for Research & Innovation, “Ministry of Education” in Saudi Arabia for funding this research work through the project number IFKSURG-1440-141.

Conflicts of Interest: The authors declare no conflict of interest.

References

1. Avci, D.; Tamer, Ö.; Başoğlu, A.; Atalay, Y. 5-Methyl-2-thiophenecarboxaldehyde: Experimental and TD/DFT study. *J. Mol. Struct.* **2018**, *1174*, 52–59. [[CrossRef](#)]
2. Da Silva, M.A.R.; Santos, A.F.L. Experimental thermochemical study of 3-acetyl-2-methyl-5-phenylthiophene. *J. Chem. Thermodyn.* **2010**, *42*, 128–133. [[CrossRef](#)]
3. Brugman, S.J.T.; Engwerda, A.H.J.; Kalkman, E.; De Ronde, E.; Tinnemans, P.; Vlieg, E. The crystal structures of four dimethoxybenzaldehyde isomers. *Acta Crystallogr. Sect. E Crystallogr. Commun.* **2019**, *75*, 38–42. [[CrossRef](#)]

4. Ma, C.; Liu, S.; Zhang, S.; Xu, T.; Yu, X.; Gao, Y.; Zhai, C.; Li, C.; Lei, C.; Fan, S.; et al. Evidence and perspective for the role of the NLRP3 inflammasome signaling pathway in ischemic stroke and its therapeutic potential (Review). *Int. J. Mol. Med.* **2018**, *42*, 2979–2990. [[CrossRef](#)]
5. Atta, A.K.; Kim, S.-B.; Cho, D.-G. Catalytic Oxidative Conversion of Aldehydes to Carboxylic Esters and Acids under Mild Conditions. *Bull. Korean Chem. Soc.* **2011**, *32*, 2070–2072. [[CrossRef](#)]
6. Hodgson, D.M.; Charlton, A. Methods for direct generation of α -alkyl-substituted aldehydes. *Tetrahedron* **2014**, *70*, 2207. [[CrossRef](#)]
7. Ding, Y.-Q.; Cui, Y.; Li, T.-D. New Views on the Reaction of Primary Amine and Aldehyde from DFT Study. *J. Phys. Chem. A* **2015**, *119*, 4252–4260. [[CrossRef](#)] [[PubMed](#)]
8. Arjunan, V.; Santhanam, R.; Rani, T.; Rosi, H.; Mohan, S. Conformational, vibrational, NMR and DFT studies of N-methylacetanilide. *Spectrochim. Acta Part A Mol. Biomol. Spectrosc.* **2013**, *104*, 182–196. [[CrossRef](#)] [[PubMed](#)]
9. Sevvanthi, S.; Muthu, S.; Raja, M. Molecular docking, vibrational spectroscopy studies of (RS)-2-(tert-butylamino)-1-(3-chlorophenyl)propan-1-one: A potential adrenaline uptake inhibitor. *J. Mol. Struct.* **2018**, *1173*, 251–260. [[CrossRef](#)]
10. Barakat, A.; Islam, M.S.; Al-Majid, A.M.; Ghabbour, H.A.; Atef, S.; Zarrouk, A.; Warad, I.; Gu, Y.; Liu, Y. Quantum chemical insight into the molecular structure of L-chemosensor 1,3-dimethyl-5-(thien-2-ylmethylene)-pyrimidine-2,4,6-(1H,3H,5H)-trione: Naked-eye colorimetric detection of copper(II) anions. *J. Theor. Comput. Chem.* **2018**, *17*, 1850005. [[CrossRef](#)]
11. Barakat, A.; Soliman, S.M.; Ghabbour, H.A.; Ali, M.; Al-Majid, A.M.; Zarrouk, A.; Warad, I. Intermolecular interactions in crystal structure, Hirshfeld surface, characterization, DFT and thermal analysis of 5-((5-bromo-1H-indol-3-yl)methylene)-1,3-dimethylpyrimidine-2,4,6(1H, 3H, 5H)-trione indole. *J. Mol. Struct.* **2017**, *1137*, 354–361. [[CrossRef](#)]
12. Zi, Y.; Zhu, M.; Li, X.; Xu, Y.; Wei, H.; Li, D.; Mu, C. Effects of carboxyl and aldehyde groups on the antibacterial activity of oxidized amylose. *Carbohydr. Polym.* **2018**, *192*, 118–125. [[CrossRef](#)] [[PubMed](#)]
13. Barnsley, J.E.; Wagner, P.; Officer, D.L.; Gordon, K.C. Aldehyde isomers of porphyrin: A spectroscopic and computational study. *J. Mol. Struct.* **2018**, *1173*, 665–670. [[CrossRef](#)]
14. Meng, X.-Y.; Zhang, H.-X.; Mezei, M.; Cui, M. Molecular Docking: A Powerful Approach for Structure-Based Drug Discovery. *Curr. Comput. Drug Des.* **2011**, *7*, 146–157. [[CrossRef](#)]
15. Guedes, I.A.; Camila, S.D.M.; Dardenne, L.E. Receptor–ligand molecular docking. *Biophys. Rev.* **2014**, *6*, 75. [[CrossRef](#)]
16. Hamilton, P.L.; Arya, D.P. Natural product DNA major groove binders. *Nat. Prod. Rep.* **2011**, *29*, 134–143. [[CrossRef](#)]
17. Rehman, S.U.; Sarwar, T.; Husain, M.A.; Ishqi, H.M.; Tabish, M. Studying non-covalent drug–DNA interactions. *Arch. Biochem. Biophys.* **2015**, *576*, 49. [[CrossRef](#)]
18. Arjmand, F.; Parveen, S.; Afzal, M.; Shahid, M. Synthesis, characterization, biological studies (DNA binding, cleavage, antibacterial and topoisomerase I) and molecular docking of copper(II) benzimidazole complexes. *J. Photochem. Photobiol. B Biol.* **2012**, *114*, 15–26. [[CrossRef](#)]
19. Barnes, E.C.; Petersson, G.A.; Montgomery, J.A.; Frisch, M.J.; Martin, J.M.L.; Martin, J.M.L. Unrestricted Coupled Cluster and Brueckner Doubles Variations of W1 Theory. *J. Chem. Theory Comput.* **2009**, *5*, 2687–2693. [[CrossRef](#)]
20. Becke, A.D. Density-functional exchange-energy approximation with correct asymptotic behavior. *Phys. Rev. A* **1988**, *38*, 3098–3100. [[CrossRef](#)]
21. Perdew, J.P.; Burke, K.; Ernzerhof, M. Generalized Gradient Approximation Made Simple. *Phys. Rev. Lett.* **1996**, *77*, 3865–3868. [[CrossRef](#)] [[PubMed](#)]
22. Wolff, S.K.; Grimwood, D.J.; McKinnon, J.J.; Jayatilaka, D.; Spackman, M.A. *CrystalExplorer 2.1*; University of Western Australia: Perth, Australia, 2007.
23. Sheldrick, G. A short history of SHELX. *Acta Crystallogr. Sect. A Found. Crystallogr.* **2008**, *64*, 112–122. [[CrossRef](#)] [[PubMed](#)]
24. Trott, O.; Olson, A.J. AutoDock Vina: Improving the speed and accuracy of docking with a new scoring function, efficient optimization, and multithreading. *J. Comput. Chem.* **2009**, *31*, 455–461. [[CrossRef](#)] [[PubMed](#)]
25. Drew, H.R.; Wing, R.M.; Takano, T.; Broka, C.A.; Tanaka, S.; Itakura, K.; Dickerson, R.E. Structure of a B-DNA dodecamer: Conformation and dynamics. *Proc. Natl. Acad. Sci. USA* **1981**, *78*, 2179–2183. [[CrossRef](#)]

26. Titi, A.; Warad, I.; Almutairi, S.M.; Fettouhi, M.; Messali, M.; Aljuhani, A.; Touzani, R.; Zarrouk, A. One-pot liquid microwave-assisted green synthesis of neutral trans-Cl₂Cu(NNOH)₂: XRD/HSA-interactions, antifungal and antibacterial evaluations. *Inorg. Chem. Commun.* **2020**, *122*, 108292. [[CrossRef](#)]
27. Warad, I.; Awwadi, F.F.; Abd Al-Ghani, B.; Sawafta, A.; Shivalingegowda, N.; Lokanath, N.K.; Mubarak, M.S.; Ben Hadda, T.; Zarrouk, A.; Al-Rimawi, F.; et al. Ultrasound-assisted synthesis of two novel [CuBr(diamine)₂.H₂O]Br complexes: Solvatochromism, crystal structure, physicochemical, Hirshfeld surface thermal, DNA/binding, antitumor and antibacterial activities. *Ultraso. Sonochem.* **2018**, *48*, 1. [[CrossRef](#)]
28. Warad, I.; Musameh, S.; Sawafta, A.; Brandão, P.; Tavares, C.J.; Zarrouk, A.; Amereih, S.; Al Ali, A.; Shariah, R. Ultrasonic synthesis of Oct. trans-Br₂Cu(N ∩ N)₂ Jahn-Teller distortion complex: XRD-properties, solvatochromism, thermal, kinetic and DNA-binding evaluations. *Ultraso. Sonochemistry* **2019**, *52*, 428–436. [[CrossRef](#)]
29. Abu Saleemh, F.; Musameh, S.; Sawafta, A.; Brandao, P.; Tavares, C.J.; Ferdov, S.; Barakat, A.; Al Ali, A.; Hamani, H.; Warad, I. Diethylenetriamine/diamines/copper (II) complexes [Cu(dien)(NN)]Br 2: Synthesis, solvatochromism, thermal, electrochemistry, single crystal, Hirshfeld surface analysis and antibacterial activity. *Arab. J. Chem.* **2017**, *10*, 845–854. [[CrossRef](#)]
30. Aouad, M.R.; Messali, M.; Rezki, N.; Al-Zaqri, N.; Warad, I. Single proton intramigration in novel 4-phenyl-3-((4-phenyl-1H-1,2,3-triazol-1-yl)methyl)-1H-1,2,4-triazole-5(4H)-thione: XRD-crystal interactions, physicochemical, thermal, Hirshfeld surface, DFT realization of thiol/thione tautomerism. *J. Mol. Liq.* **2018**, *264*, 621–630. [[CrossRef](#)]
31. Tauc, J.; Mentsh, A. States in the gap. *J. Non-Cryst. Solids* **1972**, *8*, 569–585. [[CrossRef](#)]
32. Banfi, D.; Patiny, L. www.nmrdb.org: Resurrecting and Processing NMR Spectra On-line. *Chim. Int. J. Chem.* **2008**, *62*, 280–281. [[CrossRef](#)]
33. Shi, J.-H.; Lou, Y.-Y.; Zhou, K.-L.; Pan, D.-Q. Exploration of intermolecular interaction of calf thymus DNA with sulfosulfuron using multi-spectroscopic and molecular docking techniques. *Spectrochim. Acta Part A Mol. Biomol. Spectrosc.* **2018**, *204*, 209–216. [[CrossRef](#)] [[PubMed](#)]

Sample Availability: Samples of the compounds are available from the authors.

Publisher's Note: MDPI stays neutral with regard to jurisdictional claims in published maps and institutional affiliations.



© 2020 by the authors. Licensee MDPI, Basel, Switzerland. This article is an open access article distributed under the terms and conditions of the Creative Commons Attribution (CC BY) license (<http://creativecommons.org/licenses/by/4.0/>).